10th Oxford School on Neutron Scattering

4-14 September 2007

University of Oxford, Mansfield College

ANSWER BOOK

CONTENTS

Supported by:

ISIS NEUTRONS FOR SCIENCE nmi3

http://www.oxfordneutronschool.org/

A. Single-Crystal Diffraction

A1.

(i) From the relation $\lambda = h/(m_n \mathrm{v}_n)$ we get

$$\lambda \text{ (Å)} = 3.956/\mathrm{v}_n (km/\text{sec}).$$

Putting v_n=2.20 *km/sec* gives λ=**1.798 *Å***.

(ii) Similarly from $E = \frac{1}{2} m_n \mathrm{v}_n^2$ we obtain *E*= **25.30 *meV***.

(iii) The X-ray energy is given by:

$$E_X = h\nu = \frac{hc}{\lambda}$$

with ν the frequency of the X-rays and c the velocity of light.
Putting $c = 2.998 x 10^8 \, m/sec$ and $\lambda = 1.8 x 10^{-10} \, m$ gives

$$E = \textbf{6.88 kV}$$

(iv) The velocity of a neutron with this energy is

$$\mathrm{v}_n = \left(\frac{2E}{m_n} \right)^{1/2},$$

i.e. v_n= **1148*km/sec***

We see then that thermal neutrons have both wavelengths suitable for studying atomic structures in the 1-100Å range and energies suitable for studying excitations (such as phonons or magnons) in the meV-eV range. (Fast neutrons have too short a wavelength and are too energetic for either purpose.)

A2

(i). The wavelength of the reflected beam is

$$\lambda = 2d_{111}\sin\theta$$

where $d_{111} = \frac{a_0}{\sqrt{3}} = 2.85\text{Å}$. Thus $\sin\theta = 1.8/5.7$ and the scattering angle is

$$2\theta = \underline{\mathbf{36.7}}\ ^{\mathbf{o}}\ .$$

(ii). The wavelength spread is derived by differentiating Bragg's equation:

$$\frac{\Delta\lambda}{\lambda} = -\cot\theta.\Delta\theta \quad .$$

Putting $\Delta\theta = 0.2^{\circ}$ gives $\frac{\Delta\lambda}{\lambda} = 0.0105$, so that for $\lambda = 1.8\text{Å}$ we get

$$\Delta\lambda = \underline{\pm\mathbf{0.019}\text{Å}}$$

Note that this spread of wavelengths is much larger than the natural width of characteristic X-ray lines, and so Bragg peaks obtained with neutrons will not be as sharp as X-ray peaks.

A3

Figure A1 shows the reciprocal lattice in the $\mathbf{a}^*\mathbf{b}^*$ plane, together with the Ewald circles passing through the reflections *630* and *360* .

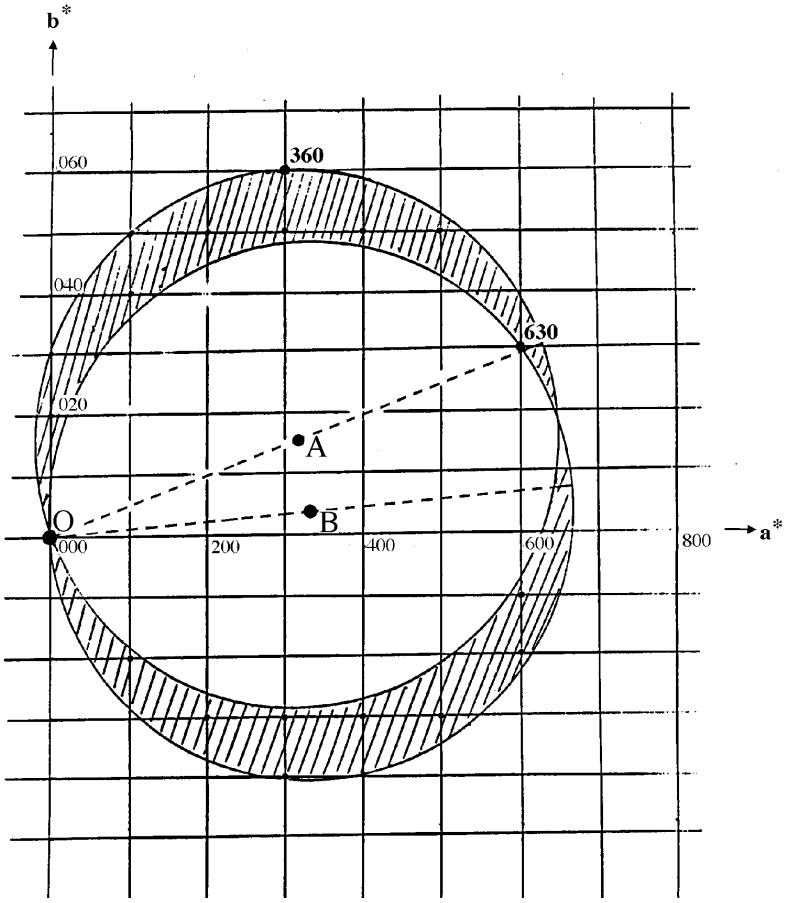

Figure A1. The Ewald circles for the *630* and *360* reflections. A is the centre of the circle for *360* and B is the centre of the circle for *630*.

We can consider the crystal to be stationary and the incident beam to turn between the directions $\mathbf{AO}\rightarrow$ and $\mathbf{BO}\rightarrow$ in the Figure. During this rotation the area swept out in reciprocal space is the shaded region. The number of reciprocal lattice points in this region, i.e. the number of Bragg reflections, is approximately 18.

A4

Figure A2 shows the Ewald circles drawn for the two extreme wavelengths. The observable reflections are those lying in the shaded area lying between the two circles. For a primitive unit cell there are no systematically absent reflections, and so the number of possible reflections is about sixty.

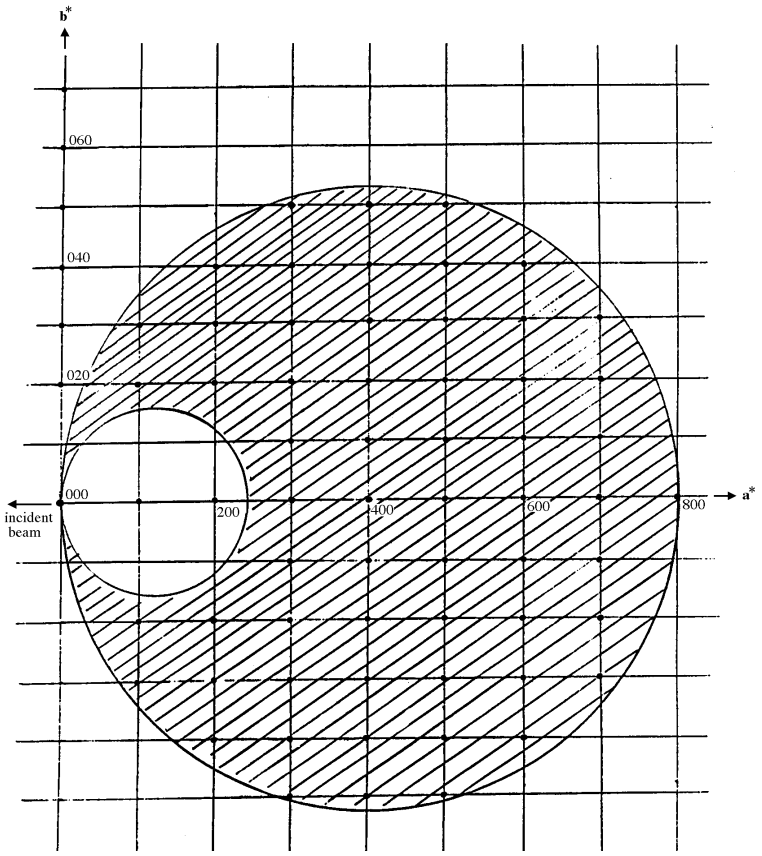

Figure A2. The Ewald construction showing the reflection circles for the minimum wavelength (maximum radius) and the maximum wavelength (minimum radius).

B. Coherence and Incoherence

B1

(1) Hydrogen.

b^{coh} is derived by averaging the scattering length over the states with parallel and antiparallel neutron-nucleus spins:

$$b^{coh} = w^{+}b^{+} + w^{-}b^{-} \qquad \text{(B1a)}$$

The weights are given by $w^{+} = (I+1)/(2I+1)$ and $w^{-} = I/(2I+1)$. Putting $I = \frac{1}{2}$ we have $w^{+} = \frac{3}{4}$ and $w^{-} = \frac{1}{4}$. From Table B1:

$$b^{coh} = \left[\frac{3}{4}(1.085) + \frac{1}{4}(-4.75)\right].10^{-14}\,m$$

$$= \underline{\mathbf{-0.373\ .10^{-14}}\,m}.$$

The coherent scattering cross section is:

$$\sigma_{coh} = 4\pi\left(b^{coh}\right)^{2}. \qquad \text{(B2a)}$$

Hence σ_{coh} = **1.75 x** $10^{-28}\,m^{2}$.

The total cross section is obtained by summing the weighted values of the spin
states of the combined nucleus-neutron system:

$$\sigma_{tot} = 4\pi\left[w^{+}\left(b^{+}\right)^{2} + w^{-}\left(b^{-}\right)^{2}\right]. \qquad \text{(B3a)}$$

Hence σ_{tot} = **81.97 x** $10^{-28}\,m^{2}$**.**

Finally, the incoherent scattering cross section is the difference of σ_{tot} and σ_{coh}:

$$\sigma_{incoh} = \sigma_{tot} - \sigma_{coh}, \qquad \text{(B4a)}$$

so that $\sigma_{incoh} = \underline{\mathbf{80.23\ x}\ 10^{-28} m^2}$**.**

(2) Deuterium.

For $I = 1$ we have $w^+ = \frac{2}{3}$ and $w^- = \frac{1}{3}$. Using the data in Table B.1, eqns (B1a) to (B4a) give:

$$b^{coh} = \underline{\mathbf{+0.668\ x}\ 10^{-14} m}$$

$$\sigma_{coh} = \underline{\mathbf{5.60\ x}\ 10^{-28} m^2}$$

$$\sigma_{tot} = \underline{\mathbf{7.65\ x}\ 10^{-28} m^2}$$

$$\sigma_{incoh} = \underline{\mathbf{2.04\ x}\ 10^{-28} m^2}$$

B2

In this example the incoherent scattering is mainly due to the isotope effect but there is a small contribution from the spin effect.

The coherent scattering length is the weighted average of the scattering lengths of the different isotopes:

$$b^{coh} = \sum_r c_r \left(w_r^+ b_r^+ + w_r^- b_r^- \right)$$

Using Table B.1a below we have:

$$b^{coh} = \underline{\mathbf{1.034\ x}\ 10^{-14} m}$$

The coherent scattering cross section of the element is:

$$\sigma_{coh} = 4\pi\left(b^{coh}\right)^2,$$

$$= \underline{\mathbf{13.43\ x}\ 10^{-28} m^2}\mathbf{.}$$

The total scattering cross section is:

$$\sigma_{tot} = 4\pi\sum_r c_r\left[w_r^+\left(b_r^+\right)^2 + w_r^-\left(b_r^-\right)^2\right],$$

where $$w_r^+ = \frac{I_r + 1}{2I_r + 1} \text{ and } w_r^- = \frac{I_r}{2I_r + 1}\ .$$

$$\text{i.e. } \sigma_{tot} = \underline{\mathbf{18.50\ x}\ 10^{-28} m^2}\mathbf{.}$$

Finally from the expression $\sigma_{incoh} = \sigma_{tot} - \sigma_{coh}$ we find that

$$\sigma_{incoh} = \underline{\mathbf{5.09\ x}\ 10^{-28} m^2}\mathbf{.}$$

Table B.1a

isotope r	spin I	$w_r^+ b_r^+$ $(10^{-14} m)$	$w_r^- b_r^-$ $(10^{-14} m)$	$w_r^+\left(b_r^+\right)^2$ $(10^{-28} m^2)$	$w_r^-\left(b_r^-\right)^2$ $(10^{-28} m^2)$
58	0	0.983	0	1.416	0
60	0	0.073	0	0.020	0
61	3/2	0.288	0.473	0.132	0.595
62	0	0.031	0	0.027	0

64	0	0.000	0	0.000	0

C. Time-of-Flight Powder Diffraction

C1.

(a) The expression

$$t = \left(\frac{m_{\mathrm{n}}}{h}\right)\lambda L$$

follows from the relations

$$L = \mathrm{v}t$$

$$\lambda = \frac{h}{m_n \mathrm{v}}$$

where v is the neutron velocity.

From the values of h and m_n on page 2 we get

$t(in\ \mu secs) = 252.8\lambda(in\ \text{Å})$ x $L(in\ metres)$. (C1a)

(b) In Bragg scattering from lattice planes *hkl* of spacing d_{hkl} the wavelength of the scattered radiation is given by

$$\lambda = 2d_{hkl}\sin\theta \qquad \text{(C2a)}$$

where 2θ is the scattering angle.

Putting $L = 100m$ into eqn. (C1a) and $\theta = 85^\circ$ into eqn. (C2a) gives

$$t(\mu sec\, s) = 5.036 \times 10^4\, d_{hkl}\,(\text{Å}) \qquad \text{(C3a)}$$

Perovskite has a primitive cubic lattice, so that the first three Bragg reflections (corresponding to the longest times-of-flight) are *100*, *110* and *111*. Also the d-spacing is related to the lattice constant a_0 by

$$d_{hkl} = \frac{a_0}{\sqrt{\left(h^2 + k^2 + l^2\right)}}, \qquad \text{(C4a)}$$

and so $d_{100} = 3.84\text{Å}$, $d_{110} = 2.72\text{Å}$ and $d_{111} = 2.22\text{Å}$. Substituting into eqn (C3a) we find that $t_{100} = 194m\sec$, $t_{110} = 137m\sec$ and $t_{111} = 112m\sec$.

(c) Combining eqns. (C3a) (C4a) gives:

$$t \propto \left(h^2 + k^2 + l^2\right)^{-1/2}. \qquad \text{(C5a)}$$

C2.

(a) The *Structure Factor* F_{hkl}, or the amplitude of the scattering into the *hkl* Bragg reflection by the atoms in one unit cell, is given by:

$$F_{hkl} = \sum_{j=1}^{N} b_j \exp\left\{2\pi i\left(hx_j + ky_j + lz_j\right)\right\}. \qquad \text{(C6a)}$$

Here b_j is the scattering length of the j^{th} nucleus in the cell, x_j y_j z_j are its fractional coordinates, and N is the total number of atoms in the cell.

In the diamond structure of silicon there is a basis of two silicon atoms at

$$000;\ \tfrac{1}{4}\tfrac{1}{4}\tfrac{1}{4}$$

and this basis is distributed at each of the face-centred-cubic lattice points:

$$000;\ \tfrac{1}{2}\tfrac{1}{2}0;\ \ \tfrac{1}{2}0\tfrac{1}{2};\ 0\tfrac{1}{2}\tfrac{1}{2}.$$

Hence N=8 and the fractional coordinates are

$$000;\ \tfrac{1}{2}\tfrac{1}{2}0;\ \ \tfrac{1}{2}0\tfrac{1}{2};\ 0\tfrac{1}{2}\tfrac{1}{2} \quad \text{for } j\text{=1 to 4}$$

and $$\tfrac{1}{4}\tfrac{1}{4}\tfrac{1}{4} \ + \left(000;\ \tfrac{1}{2}\tfrac{1}{2}0;\ \ \tfrac{1}{2}0\tfrac{1}{2};\ 0\tfrac{1}{2}\tfrac{1}{2}\right) \text{ for } j\text{=5 to 8.}$$

Inserting these coordinates into eqn. (C6a) gives:

$$F_{hkl} = b_j \left\{1 + \exp\left[\pi i(h+k)\right] + \exp\left[\pi i(h+l)\right] + \exp\left[\pi i(k+l)\right]\right\} \times \left\{1 + \exp\left[\pi i\left(\frac{h+k+l}{2}\right)\right]\right\}. \qquad \text{(C7a)}$$

If all indices are even integers the first bracket {} is equal to 4; similarly, if all indices are odd integers. If only one index is even, the first bracket {} is zero; similarly, if only one index is odd.

(b) A further restriction on the indices of the Bragg reflections is imposed by the second bracket {} in eqn. (C7a). If $\left(\frac{h+k+l}{2}\right)$ is even, this bracket is equal to 2; if $\left(\frac{h+k+l}{2}\right)$ is odd, the bracket is zero.

(c)

(i) The possible values of *hkl* for the f.c.c. lattice are shown in Table C.1a.

Table C.1a Sums of three squared integers/ Miller indices.

$h^2+k^2+l^2$ / *hkl*	$h^2+k^2+l^2$ / *hkl*	$h^2+k^2+l^2$ / *hkl*	$h^2+k^2+l^2$ / *hkl*	$h^2+k^2+l^2$ / *hkl*
1	11* 311	21	33	43* 533
2	12* 222	22	34	44* 622
3* 111	13	24* 422	35* 531	45
4* 200	14	25	36* 600/442	46
5	16* 400	26	37	48* 444
6	17	27* 511/333	38	49
8* 220	18	29	40* 620	50
9	19* 331	30	41	51* 711/551
10	20* 420	32* 440	42	52* 640

(ii) The forbidden reflections are: 200, 222, 420, 600, 442, 622, 640.

(iii) The overlapping reflections are: 511/333; 711/551.

(d) Putting $L = 14m$ into eqn. (C1a) and $\theta = 83.5^\circ$ into eqn. (C2a) gives

$$t(\mu sec\, s) = 7033 d_{hkl}(\text{Å}) \quad . \qquad \text{(C5a)}$$

and from eqns(C3a) and (C4a):

$$\frac{1}{t^2} \propto h^2 + k^2 + l^2 \quad . \qquad \text{(C6a)}$$

111 is the Bragg peak with the longest flight time. The next peak is *220* (*200* is forbidden). Thus *220* is peak no 1 in Figure C.1. Using the information in section (c) the remaining peaks are readily indexed (see Table C.1a below).

Using eqn. (C5a) we get the cell size of $a_0 = 5.4307\,\text{Å}$.

Table C.1a

peak number	time of flight ($\mu secs$)	indices *hkl*
1	13 503	220
2	11 515	311
3	9 549	400
4	8 760	331
5	7 796	422
6	7 351	511/333
7	6 753	440
8	6 455	531
9	6 038	620
10	5 823	533
11	5 512	444
12	5 348	711/551

D. Magnetic Elastic Scattering

D1.

There are 4 Mn atoms and 4 O atoms in the chemical unit cell. The structure factor for nuclear scattering is:

$$F_{nucl}^{hkl} = \sum_{j=1}^{8} b_j \exp[2\pi i(hx_j + ky_j + lz_j)]$$

$$= b_{Mn}[1 + \exp \pi i(h+k) + \exp \pi i(k+l) + \exp \pi i(l+h)]$$
$$+ b_O[\exp \pi ih + \exp \pi ik + \exp \pi il + \exp \pi i(h+k+l)] \ ,$$

where b_{Mn} and b_O are the coherent nuclear scattering lengths of the Mn and O ions. If the indices hkl are mixed (i.e. both odd and even), F_{nucl}^{hkl} is zero: the only allowed reflections are those with hkl all odd or all even. These reflections are

111, 200, 220, 311, 222, 400 .....

and they are indexed in the enlarged magnetic cell as

222, 400, 440, 622, 444, 800 .....

To calculate the magnetic structure factor F_{mag}^{hkl} we need to consider only the magnetic atoms (Mn), of which there are 32 in the magnetic cell. F_{mag}^{hkl} is given by

$$F_{mag}^{hkl} = \sum_{j=1}^{32} \pm p \exp[2\pi i(hx_j + ky_j + lz_j)] \ , \qquad \text{(D1a)}$$

where $+p$ refers to parallel spins and $-p$ to antiparallel spins. The quantities x_j, y_j, z_j in eqn. (D1a) now represent the fractional coordinates in the *enlarged* cell. These coordinates are:

$$+000;\ -\tfrac{1}{2}00;\ -0\tfrac{1}{2}0;\ -00\tfrac{1}{2};$$
$$-\tfrac{1}{4}\tfrac{1}{4}0;+\tfrac{3}{4}\tfrac{1}{4}0;\ +\tfrac{1}{4}\tfrac{3}{4}0;+\tfrac{1}{4}\tfrac{1}{4}\tfrac{1}{2};$$
$$-\tfrac{1}{4}0\tfrac{1}{4};+\tfrac{3}{4}0\tfrac{1}{4};\ +\tfrac{1}{4}\tfrac{1}{2}\tfrac{1}{4};+\tfrac{1}{4}0\tfrac{3}{4};$$
$$-0\tfrac{1}{4}\tfrac{1}{4};+\tfrac{1}{2}\tfrac{1}{4}\tfrac{1}{4};\ +0\tfrac{3}{4}\tfrac{1}{4};+0\tfrac{1}{4}\tfrac{3}{4}.$$

$$+\tfrac{1}{2}\tfrac{1}{2}0;+\tfrac{1}{2}0\tfrac{1}{2};+0\tfrac{1}{2}\tfrac{1}{2};-\tfrac{1}{2}\tfrac{1}{2}\tfrac{1}{2};$$
$$-\tfrac{3}{4}\tfrac{3}{4}0;-\tfrac{3}{4}\tfrac{1}{4}\tfrac{1}{2};-\tfrac{1}{4}\tfrac{3}{4}\tfrac{1}{2};+\tfrac{3}{4}\tfrac{3}{4}\tfrac{1}{2};$$
$$-\tfrac{3}{4}\tfrac{1}{2}\tfrac{1}{4};-\tfrac{3}{4}0\tfrac{3}{4};-\tfrac{1}{4}\tfrac{1}{2}\tfrac{3}{4};+\tfrac{3}{4}\tfrac{1}{2}\tfrac{3}{4};$$
$$-\tfrac{1}{2}\tfrac{3}{4}\tfrac{1}{4};-\tfrac{1}{2}\tfrac{1}{4}\tfrac{3}{4};-0\tfrac{3}{4}\tfrac{3}{4};+\tfrac{1}{2}\tfrac{3}{4}\tfrac{3}{4}.$$

The coordinates have been labelled as positive for parallel spins, and as negative for antiparallel spins. (We see from Figure D.1 that $x_j + y_j + z_j = 1$ for parallel spins and $x_j + y_j + z_j = \frac{1}{2}$ for antiparallel spins.) Substituting the coordinates of the Mn ions into eqn (D1a) leads to

$$F_{mag}^{hkl} = \left[1 - \exp\left(2\pi i \frac{h+k}{4}\right) - \exp\left(2\pi i \frac{k+l}{4}\right) - \exp\left(2\pi i \frac{l+h}{4}\right)\right]$$

$$\times \left[\begin{array}{l} 1 - \exp\left(2\pi \mathrm{i} \frac{\mathrm{h}}{2}\right) - \exp\left(2\pi \mathrm{i} \frac{\mathrm{k}}{2}\right) - \exp\left(2\pi \mathrm{i} \frac{\mathrm{l}}{2}\right) \\ + \exp\left(2\pi \mathrm{i} \frac{\mathrm{h}+\mathrm{k}}{2}\right) + \exp\left(2\pi \mathrm{i} \frac{\mathrm{k}+\mathrm{l}}{2}\right) \\ + \exp\left(2\pi \mathrm{i} \frac{\mathrm{l}+\mathrm{h}}{2}\right) - \exp\left(2\pi \mathrm{i} \frac{\mathrm{h}+\mathrm{k}+\mathrm{l}}{2}\right) \end{array}\right]. \qquad \text{(D2a)}$$

The second square bracket in eqn. (D2a) is zero when *h, k, l* are all even. But this is just the condition for the appearance of the nuclear reflections. Hence the two kinds of reflection are separated from one another in reciprocal space.

D2.

If the scattering vector is along $[h_1 k_1 l_1]$ and the spin direction along $[h_2 k_2 l_2]$ then the angle between them is given by:

$$\cos\alpha = \frac{h_1 h_2 + k_1 k_2 + l_1 l_2}{\sqrt{\left(h_1^2 + k_1^2 + l_1^2\right)}\sqrt{\left(h_2^2 + k_2^2 + l_2^2\right)}} \quad .$$

Using this expression we get:

$100 \wedge 111 = 54.74^\circ; \quad 100 \wedge 311 = 25.24^\circ; \quad 111 \wedge 311 = 29.49^\circ$.

In magnetic scattering we measure those components of magnetic moment which are perpendicular to the scattering vector. The existence of a *111* magnetic peak rules out the possibility of the spin direction lying along [*111*]. The more likely spin direction is along [*100*].

D3.

The cell is primitive and so there are no systematic absences (such as those encountered in Exercise C with silicon). We can therefore list the possible values of *hkl* as those given in the first column of Table **D1a** overleaf.

The d-spacings of a tetragonal crystal are given by the formula

$$(l/d)^2 = (h/a)^2 + (k/a)^2 + (l/c)^2$$

where *hkl* are the Miller indices and *a*, *c* are the dimensions of the chemical cell. The second column of the Table gives the *d*-spacings of the chemical cell, as calculated using *a*=4.874Å and *c*=3.310Å.

Table D1a

hkl	calculated *d*-spacings of chemical cell (Å)	observed *d*-spacings of chemical cell (Å)	observed *d*-spacings of magnetic cell (Å)
100	4.874	—	4.873
110	3.446	3.446	—
001	3.311	—	—
101	2.739	2.738	—
200	2.437	2.437	—
111	2.388	2.388	2.388
210	2.180	2.180	2.180

The third column gives the observed *d*-spacings of the chemical cell. The *001* reflection is not observed, because in the rutile structure half the planes of atoms normal to [*001*] scatter out-of-phase with the other half (see Figure D1a). The *100* reflection is absent for the same reason.

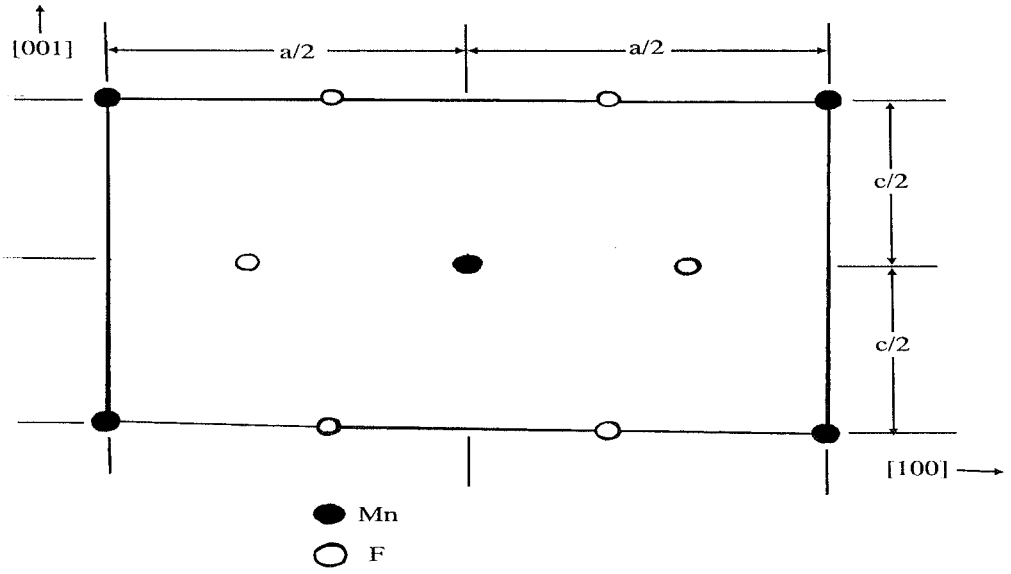

Figure D1a. Projection of atoms in *ac* plane. The atoms at cell height $z=c/2$ are out of phase with those at $z=0$.

The fourth column in the Table includes the observed *d*-spacings of the three magnetic reflections. They appear at the *100*, *111* and *210* positions of the chemical cell. It follows that (in contrast to the case of MnO in question D1) the magnetic unit cell has the same dimensions as the chemical unit cell. It also follows that the magnetic structure is commensurate with the chemical structure.

The magnetic configuration can be inferred from the presence of the *100* reflection. There are just two Mn atoms in the cell and by giving them opposite magnetic moments, as shown in Figure D2a, we obtain an antiferromagnetic configuration. The half planes of atoms at $x=0$ and $x=a/2$ now scatter in phase to produce a strong magnetic *100* reflection.

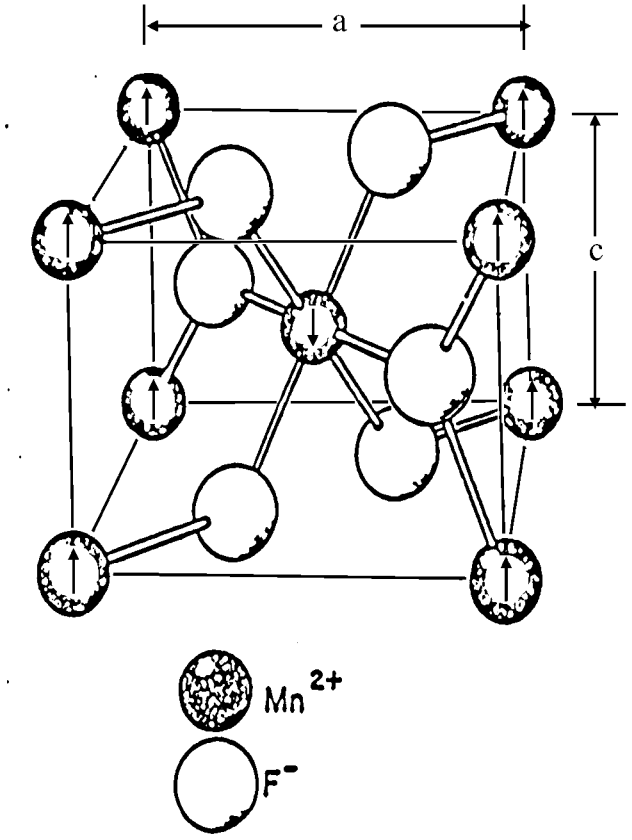

Figure D2a. Magnetic structure of MnF_2.

Finally, the absence of a magnetic *001* reflection leads uniquely to a spin alignment that is parallel to the tetragonal axis.

E. Incoherent Inelastic Scattering (with a Pulsed Neutron Spectrometer)

E1.

(i) The elastic peak in Figure E.2 occurs at the t.o.f.:

$$t \approx 64.1ms \quad .$$

The total flight path is 36.54m +1.47m=38.01m , and so the neutron velocity is

$$\mathrm{v_n} = 0.593kms^{-1}$$

and the energy selected by the crystal analyser is

$$E_n = \tfrac{1}{2} m_\mathrm{n} \mathrm{v_n}^2 = \underline{\mathbf{1.85\ meV}}\ .$$

(ii) The Bragg angle θ_A of the analyser is given by

$$\theta_A = \arcsin\left(\frac{\lambda}{2d_{002}}\right) ,$$

where $\lambda = \dfrac{h}{m_\mathrm{n}\mathrm{v_n}}$ = 6.67Å . Thus $\underline{\theta_A \approx \mathbf{85}^\circ}$.

(iii) The advantage of using a high take-off angle $\left(170^\circ\right)$ is that the wavelength band reflected by the analyser is then relatively small.

E2.

For neutron-energy gain the flight-time is greater than it is for elastic scattering, whereas for neutron-energy loss the flight-time is less than for elastic scattering. Thus the inelastic peaks in Figure E.2 are at $t \approx 65.7ms$ for energy gain and at $t \approx 62.7ms$ for energy loss.

The sample-analyser-detector distance is 1.47m and the total flight-path is 38.01m. The elastically-scattered neutrons cover the total flight path in 64.1ms, and so they cover the sample-analyser-detector distance in $64.1\text{x}(1.47/38.01)ms$ =2.48ms. The moderator-to-sample distance of 36.54m is covered by the energy-gain neutrons in the time

$$(65.7\text{-}2.48)ms = 63.2ms.$$

Hence the energy of these neutrons is

$$E_{gain} = \tfrac{1}{2} m_{\text{n}} \text{v}_{\text{n}}^2 = \tfrac{1}{2} m_{\text{n}} \left(\frac{36.54m}{63.2ms} \right)^2$$

or $E_{gain} = \underline{\mathbf{1.76}meV}$.

A similar calculation for the energy-loss neutrons gives

$$E_{loss} = \underline{\mathbf{1.94}meV} .$$

We see , therefore, that the energy transfer is $\underline{\pm\mathbf{0.09}meV}$.

E3

(i) The intensity is influenced by the Bose factor $n(E)$ which gives the number of phonons which exist at a given energy E and temperature T :

$$n(E) = \frac{1}{\exp\left(\frac{E}{k_B T}\right) - 1} \quad .$$

For neutron-energy loss the intensity is proportional to $[1 + n(E)]$, whereas for neutron-energy gain it is proportional to $n(E)$. At low temperatures $n(E)$ tends to zero and only scattering with neutron energy loss ('down scattering') is possible. There is always a greater possibility, at any temperature, that neutrons will be scattered with energy loss.

F. Coherent Inelastic Scattering (with a Triple-Axis Spectrometer)

F1.

The allowed points have *hkl* indices, which are all odd or all even. See Figure F.1a.

F2.

The relation between neutron energy *E* and neutron wave number *k* is

$$E(meV) = 2.072\left[k(\mathring{A}^{-1})\right]^2 \quad .$$

Putting $E_i^{\min} = 3meV$ and $E_i^{\max} = 14meV$ gives

k_i^{min} =**1.203** $\mathring{A}^{-1}$ and k_i^{max} =**2.600** $\mathring{A}^{-1}$..

We also have $k = 2\pi/\lambda$, so that k_i^{min} corresponds to the maximum wavelength λ_i^{max} = **5.22 Å**, and k_i^{max} to the minimum wavelength λ_i^{min} = **2.42 Å**.

F3

(i) We have $Q_{220} = 2\pi/d_{220} = \sqrt{8}\,(2\pi/a_0)$, so that Q_{220} = **3.20 Å**.

Figure F1a shows the vectors $\mathbf{k}_i$, $\mathbf{k}_f$, and **Q** for the *220* reflection.

(ii) Putting $k_i = k_f$ into $Q^2 = k_i^2 + k_f^2 - 2k_i k_f \cos\phi$ we get
$\phi = 2\sin^{-1}(Q/2k_i)$,

and so ϕ=**75.9 º**.

(iii) In the case of elastic scattering the scattering angle ϕ is twice the Bragg angle θ_B.

F4.

See Figure F1a.

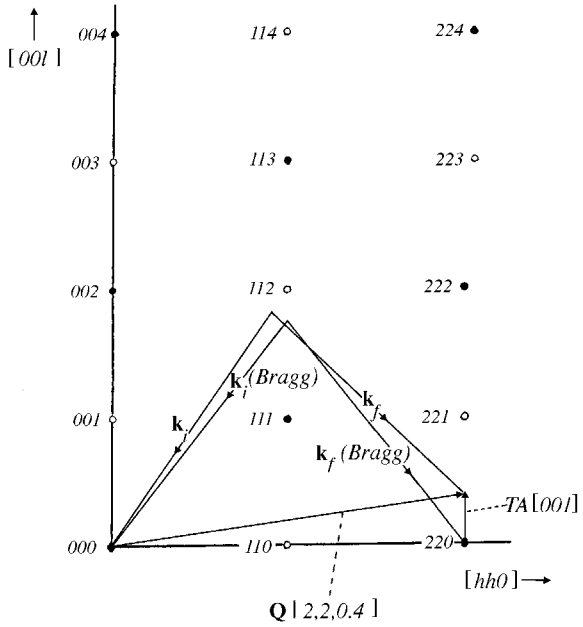

Figure F.1a. Reciprocal lattice construction for *220* Bragg scattering and for inelastic scattering by the transverse acoustic [*001*] phonon.

F5.

The vector **Q**[*2, 2, 0. 4*] (Figure F1a) is of magnitude

$$Q = 2\pi / a_0 \,.\sqrt{4+4+0.16} = 3.228\,\mathring{A}^{-1}.$$

We have $E_i^{\max} = 14 meV$ and $\Delta E = 3 meV$. Hence for neutron energy

loss $E_f = 11meV$ and for neutron energy gain $E_f = 17meV$. Using eqn. (F4) of *Exercises F* we get $k_f = 2.304\AA^{-1}$ for energy loss and $k_f = 2.864\AA^{-1}$ for energy gain. From eqn. (F2) we then have $\phi = 82.1^\circ$ (loss) and $\phi = 72.2^\circ$ (gain) .

F6.

The resolution is best for small k_f, i.e. for energy loss. In Figure F.1* the vectors $\mathbf{k}_i$ and $\mathbf{k}_f$ are drawn for this configuration.

F7.

(i) At 300*K*: $n(E)$=8.3 for energy gain and $n(E) + 1 = 9.3$ for energy loss.
At 0*K*: $n(E)$=0 for energy gain and $n(E) + 1 = 1$ for energy loss.

(ii) Thus it doesn't make much difference at 300*K* whether one works in energy gain or in energy loss, but at low temperatures one must work in energy loss.

F8.

No; not with this value of the incident wavelength. We have $Q_{440} = 2Q_{220}$ $=6.46\AA^{-1}$, $k_i + k_f = 4.904\AA^{-1}$ in energy loss , and $k_i + k_f = 5.464\AA^{-1}$ in energy gain. Hence $k_i + k_f < Q$ and it is impossible to close the scattering triangle (Figure F.2) in either case.

G: Disordered Materials Diffraction

Exercise G 1

G 1.1a) & c)

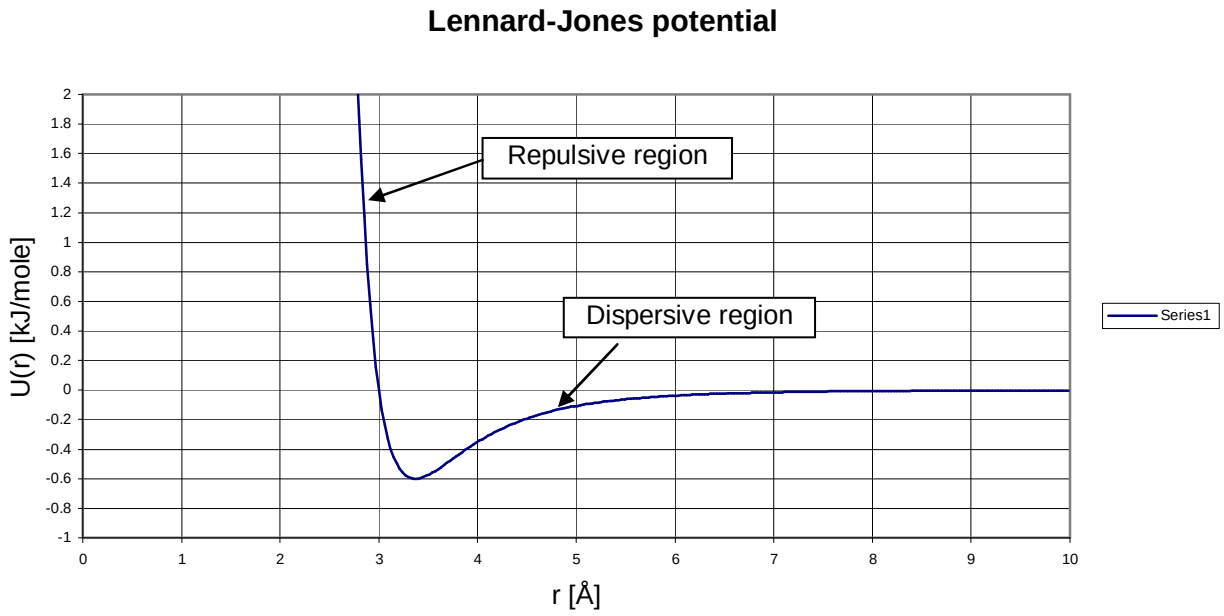

G 1.1b) εrepresents the depth of the potential. It controls how tightly adjacent atoms are bound. σ represents the radius at which the hard core repulsive region goes to zero. It represents roughly the distance of closest approach of two atoms.

G 1.1a)

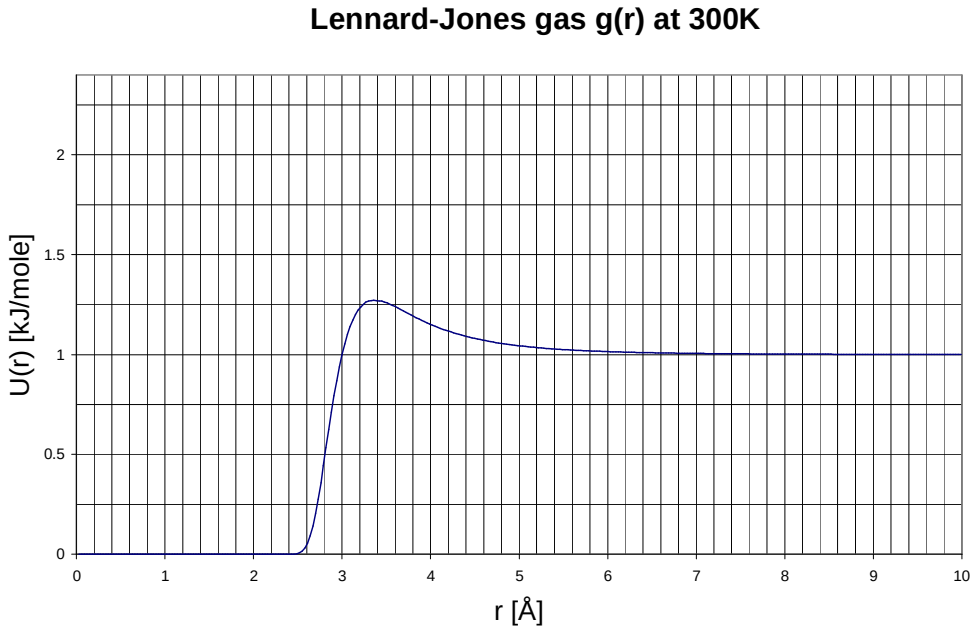

G 1.2b) At low r, $U(r)$ becomes very large, while $g(r)$ goes to zero. At high r, $U(r)$ goes to zero, while $g(r)$ goes to unity. In between the two functions are in rough antiphase.

G 1.2c) If ε were increased by a factor of 2, the height of the peak in $g(r)$ at ~ 3.8Å would grow from ~1.27 to ~1.54. If σ were increased by 20%, the main peak would move out by 20%, but would remain the same height.

G 1.3a) In the gas form $g(r)$ decays monotonically to unity at large r. As the density increases the height of the main peak increases and it becomes sharper as a series of decaying oscillations occurs towards larger r. All the peaks move to smaller r with increasing density.

Based on a change of density of 0.02 to 0.035, one might expect the separation of peaks to change by the cube root of the ratio of densities, namely $\sqrt[3]{0.02/0.035} = 0.83$. In fact the first peak moves from 3.18Å to 3.06Å, a fractional change of only 0.96, while the second peak moves from 6.39Å to 5.91Å, a fractional change of 0.92. In other words the peaks in $g(r)$ do NOT represent the mean separation of the atoms.

G 1.3b) Why many body effects have the effect they do is the million dollar question – if only we knew the answer! Fundamentally as the material becomes more dense the direct interactions between atoms 1 and 2 become increasingly affected by the presence of 3rd, 4th , etc. atoms which increasingly surround them, and which increasingly confine them in space. Within the pairwise additive approximation assumed here all the atoms interact via known pairwise forces, but the result is many body *correlations* which are difficult to predict accurately. A raft methods to do this approximately exist, but few if any of them work for the kind of interatomic forces that are found in real materials. Hence in practice one has little option but to use computer simulation to determine the effect of many-body correlations in real materials. This problem affects crystals as much as it affects liquids, but in a crystal one has a repeat lattice (which is itself a consequence of many body correlations) which we can determine from the position and height of the Bragg peaks. In any case the primary goal of interest in crystallography is the single particle correlation function (the lattice), not the higher order correlations. The single particle correlation function for a liquid is uniform and contains no information. For a glass it is not uniform, but contains no repeat distances.

G 1.4a) For density 0.02 the first minimum occurs at 4.95Å, giving a coordination number of ~10 atoms. For density 0.035, the first minimum is at 4.47 Å with a coordination number of 12.5. Clearly these numbers do not scale with density change: coordination number varies less rapidly than the density.

G 1.4b) If instead we had used the same radius, 4.47 Å, then the coordination number at density 0.02 is 7.23, a ratio of 0.58 compared to density 0.035, which is quite close to the ratio of densities, 0.57. This illustrates again that peaks and dips in $g(r)$ do not correlate directly with the density, although they are obviously related to it.

G 1.5a) The primary effect of changing the density on the structure factor is to increase the amplitude of the oscillations. There is some movement of the peaks as well, but fundmentally as the density increases they become sharper, and the oscillations extend to large *Q*.

G 1.5b) For density 0.02, the first peak in $g(r)$ is at 3.18Å and the first peak in *S(Q)* is at 2.2Å^{-1}. For density 0.035, the first peak in $g(r)$ is at 3.06Å and the first peak in *S(Q)* is at 2.35Å^{-1}, i.e. as the peaks in $g(r)$ move in, those in *S(Q)* move out, although the movement of the first peak in *S(Q)* is more related to the movement of the 2nd and subsequent peaks in $g(r)$ than it is to the first peak in $g(r)$.

G 1.5c) It depends how we did it. If we increased σ at constant density, then the peaks would move out, but also become markedly sharper as the packing fraction of the liquid increased. If the density was reduced to compensate for the increase (atoms occupying more space) then the peaks in *S(Q)* would move in, but without increased amplitude.

G 1.5d) Since the structure factor only exists if the density is finite, a zero density will produce zero structure factor.

G 1.6d) Particular difficulties are:-

a) The data are only available over a finite *Q* range;

b) The data are multiplied by *Q* in the integrand of (1.5) making the effect of statistical uncertainty at high *Q* a particular difficulty.

c) No matter how careful they are measured and corrected, diffraction data always have systematic errors, which can seriously perturb the Fourier transform, particularly at low *r*.

The view at ISIS is that Fourier transforms should be avoided wherever possible. Instead the data should be compared with a model of the data, and then, assuming the model is satisfactory, use the model to generate the real space distributions.

Exercise G 2

G 2.1a) Atomic fractions are $c_{Zn} = 1/3 = 0.333$, $c_{Cl} = 2/3 = 0.667$

G 2.1b) $F(Q) = \frac{1}{9}\,{}^{2}b_{Zn}H_{ZnZn}(Q) + \frac{4}{9}\,b_{Zn}b_{Cl}H_{ZnCl}(Q) + \frac{4}{9}\,{}^{2}b_{Cl}H_{ClCl}(Q)$

G 2.1c) In essence the idea is that we measure $F(Q)$ for three samples, namely one with only ^{35}Cl isotope present, another with only ^{37}Cl isotope present, and a third with a mixture of x parts ^{35}Cl and (1-x) parts of ^{37}Cl. For this third sample the chlorine scattering length is $b_{mix} = xb_{^{35}Cl} + (1-x)b_{^{37}Cl}$, which means the weighting coefficient of the H_{ClCl} partial structure factor for this sample is not a linear combination of the same coefficient for the other two samples. This means the determinant of coefficients in the above formula for the three samples is finite and the matrix of coefficients can be inverted. Hence the three measurements can be used to extract the three partial structure factors, at least in principle.

A basic assumption of the isotope substitution method is that the partial structure factors do not change appreciably with isotopic composition of the sample. This is an accurate assumption in most cases, but is less accurate when hydrogen is replaced with deuterium, particularly at low temperatures and with larger molecules, because in these cases quantum effects due to the different masses can impact on both the structure and the phase diagram of the material in question.

G 2.1d) Remarkably few in practice. There have been attempts to perform isomorphic substitution with X-rays, but these method tends to be shrouded in uncertainties from knowing whether one atom can substitute for another without . Then there has been the combination of neutrons, X-rays and electrons, but each technique requires quite different sample containment, making comparisons of the three results dubious. A more promising approach is the use of anomalous dispersion of X-rays, whereby you vary the scattering length of one component near an absorption edge. This method is quite promising, but requires highly stable precision equipment to be performed satisfactorily, and to date has only be tried on a handful of materials. It suffers also from poor counting statistics because of the high degree of monochromatisation needed for the incident beam of X-rays.

G 2.2a) This is a very common problem in neutron scattering using isotopes: one or more of the components makes only a small contribution to the scattering pattern. In this case it is the *ZnZn* structure factor. Below is shown the inversion of the weights matrix:-

TABLE II
Inversion of the matrix of coefficients of Table I

Partial Structure Factor	**$Zn^{35}Cl_2$**	**$Zn^{mix}Cl_2$**	**$Zn^{37}Cl_2$**
Zn-Zn	37.25	-71.53	62.16
Zn-Cl	-21.87	39.37	-17.50
Cl-Cl	10.15	-14.99	4.84

You will notice that to extract the *ZnZn* partial structure factor we need to multiply the data by large numbers, making us rely heavily on the absolute accuracy of the diffraction data if we are to avoid amplifying systematic errors in the final structure factor. Obtaining scattering cross sections with absolute accuracies better than 1% is a tall order with any technique, including neutrons, and is rarely achieved.

G 2.2b) Fourier transform of data with potential significant systematic error is risky: the systematic error can have the effect of introducing backgrounds in real space that can make the peaks larger or smaller than they should be. As a consequence coordination numbers can be equally faulty.

G 2.2c) At ISIS we advocate, as in G 1.6d) above, the use of computer simulation to produce a model of the measured differential cross sections. This will help to identify what might be wrong with the data, and avoid some of the problems introduced by systematic effects. Some authorities dispute the use of computer simulation to achieve this, and invoke a series of consistency checks on the data analysis instead. These are used to identify and correct particular problems with the data, but this is a very time consuming process, which can take months to resolve. The net effect is the same however: in computer simulation one is already applying a series of physical consistency checks on the data, with the advantage that you have at the end a physical model of the scattering system which is consistent with your data. With the other methods, you have corrected data, but you still have the problem of trying to understand what they mean.

Without more progress in understanding the source of the systematic error it is difficult to see how these methods can be improved in the immediate future.

G 2.3a) The figure below shows the running coordination number of this *g*(*r*):-

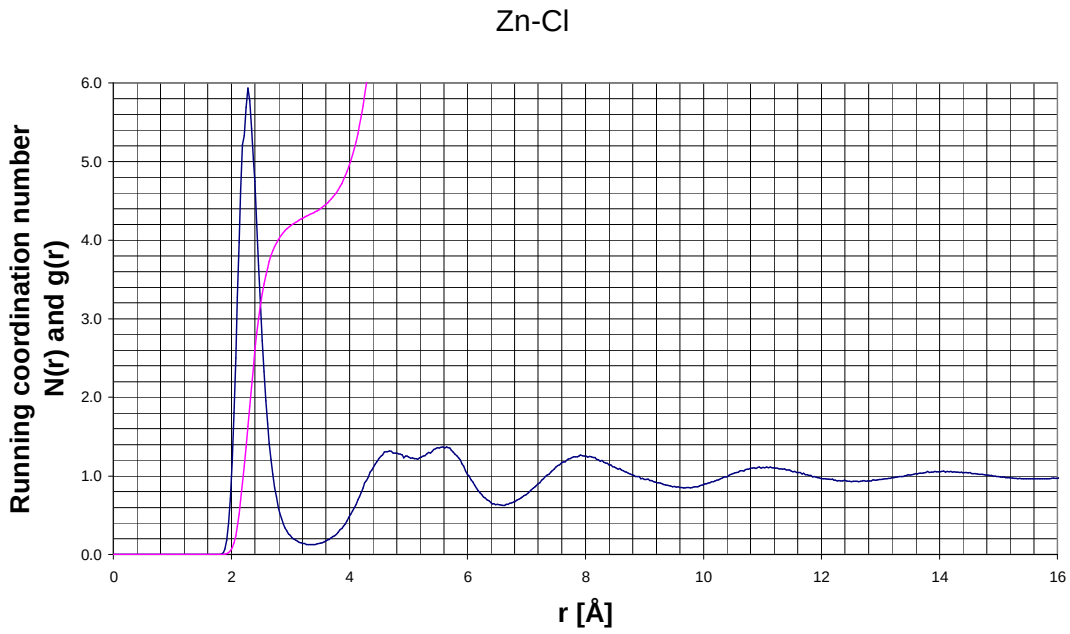

From this graph we can read that at the first minimum, 3.36Å, the running coordiation number is 4.3 *Cl* about *Zn*.

G 2.3b) The first *ZnCl* peak is at 2.31Å, while the first *ClCl* distance is at 3.69Å. Using the cosine rule, I estimate the *Cl-Zn-Cl* angle to be 106º, which is close to the tetrahedral angle of 109.47º. This together with the coordination number of 4 is a strong hint of tetrahedral local coordination in this liquid.

Taking this argument a bit further, one notices that the first *ZnZn* peak is at 3.93Å, while the second is at 6.81Å, giving a *Zn-Zn-Zn* angle of 120º, suggesting also that at least the *Zn* packing is not simple, and probably maps the tetrahedral packing of the *Cl* around *Zn*.

G 2.3c) Looking at the curves one is struck by the way the *ZnCl* oscillations are almost exactly out of phase with the *ZnZn* and *ClCl* oscillations. This strongly indicative of charge ordering, although it is not entirely clear that *Zn* and *Cl* are fully ionic in this system. Similar patterns are seen in amorphous silica, but that is very definitely not supposed to be ionic!

G 2.3d) Pass! I believe it is a clue to something fundamental about the way tetrahedral systems are organised, but at this stage I am not prepared to say what!

Exercise G 3

G 3.1a) The basic limitation is that the diffraction experiment will only probe the distribution of pair distances. It tells us nothing about the orientational correlations directly – we can only get these by surmise and (better) modelling the diffraction data. A further limitation is that it is very rare that we can by isotope substitution obtain all the relevant distributions, since many molecules contain atoms like oxygen and carbon together which have no suitable isotopes, and there is no way of separating out these important contributions. Even if the isotopes are available, it will depend on the neutron weightings as to how successful we are in any particular case in separating out the relevant pair distribution functions, as we saw in the previous exercise.

G 3.1b) Fortunately there is an escape clause. According to the theory of molecular fluids (Gray and Gubbins, Oxford,~1986) there is a spherical harmonic expansion of the orientational pair correlation function which ALSO relates to the site-site distributions. The relationship involves the calculation of a series of molecular form factors that depend on the distribution of atoms within each molecule. Thus the site-site distributions (and hence the data) *can* be sensitive to molecular orientations if the molecules themselves have the correct shape. In the past the attempt has been made to extract the orientational correlations by making use of these relationships, and using the data as constraints on the values of the spherical harmonic coefficients, and this works up to a point. This involves quite a complex use of Maximum Entropy theory. However since computer simulation is by now relatively straightforward, it much easier to simply simulate the system under investigation and then interrogate that simulation for the required orientational functions. Of course the result is not exact, but at least it helps to constrain and limit the possible orientational correlation functions.

G 3.2b) The choice of axes is usually made such as to maximise the degree of symmetry about those axes.

For H_2O one normally chooses the *z*-axis to bisect the two H atoms, with the H atoms lying in the *z*-*y* or *z*-*x* plane. This gives a 2-fold rotational symmetry about the *z*-axis and a mirror plane in the *z*-*x* plane.

For NH_3 again the *z*-axis passes through the midpoint of the three H atoms, with one of the H atoms lying in the *z*-*x* plane. This gives a 3-fold rotational symmetry about the *z*-axis and a mirror plane in the *z*-*x* plane.

CH_4 is a tetrahedral molecule, so the natural choice is for the *z*-axis to bisect 2 of the H atoms, with one of the H atoms in the *z*-*y* plane. This gives a 2-fold rotational symmetry about the *z*-axis and a mirror plane in the *z*-*x* plane. Equally a 3-fold rotational axis could be defined with the *z*-axis passing directly through one of the H atoms.

Benzene, a 6-membered ring molecule, could again be defined in several ways. Probably the easiest is to draw the *z*-axis perpendicular to the plane of the ring and passing through the centre: this axis would then have 6-fold rotational symmetry. The *x*- or *y*-axes are then defined using one of the carbon atoms.

Methanol, CH_3OH, has two possible centres, either C or O, depending on what quantity is under investigation. If we are interested in the distribution of neighbours around the methyl headgroup, then we might chose the C atom as the centre, with O atom forming the (negative) *z*-axis. If on the other hand we are interested in both headgroups, methyl and hydroxyl, we might choose the O atom as the centre, with *z*-axis bisecting the line joining the C and the hydroxyl H:-

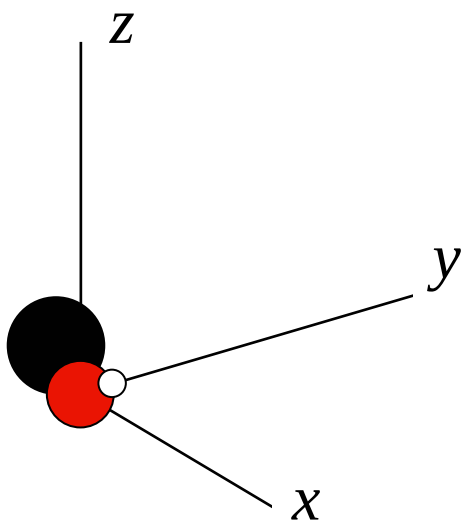

Ethanol, CH_3CH_2OH, presents a problem, since the CH_3 group can rotate about the O-CH_2 axis. Probably the easiest approach is to set the axes as for methanol above, and then average about the rotations of the CH_3 group. Clearly as molecules become increasingly "floppy" definition of suitable axes of symmetry becomes harder. In that case one would concentrate on a particular site of interest, such as the OH group in the case of ethanol.

G 3.3a) There are several answers to the question why water is so good with neutrons. Part of it of course is that isotopes H and D are available. The H isotope is particularly useful for dynamic studies since it enhances the single atom scattering considerably over the interference scattering. For diffraction the main gain is the large change in scattering length between H and D, and indeed the change in sign of the scattering length between the two isotopes, -3.74fm for H, +6.67 for D. As will be seen in the rest of this exercise, water has a very characteristic local order which, combined with its particular molecular geometry, makes it almost ideally suited to neutron diffraction with isotope substitution.

G 3.3b)

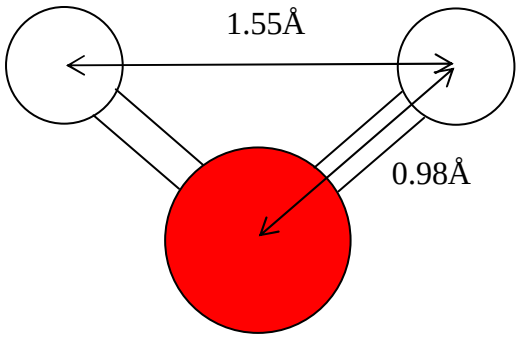

G 3.3c)

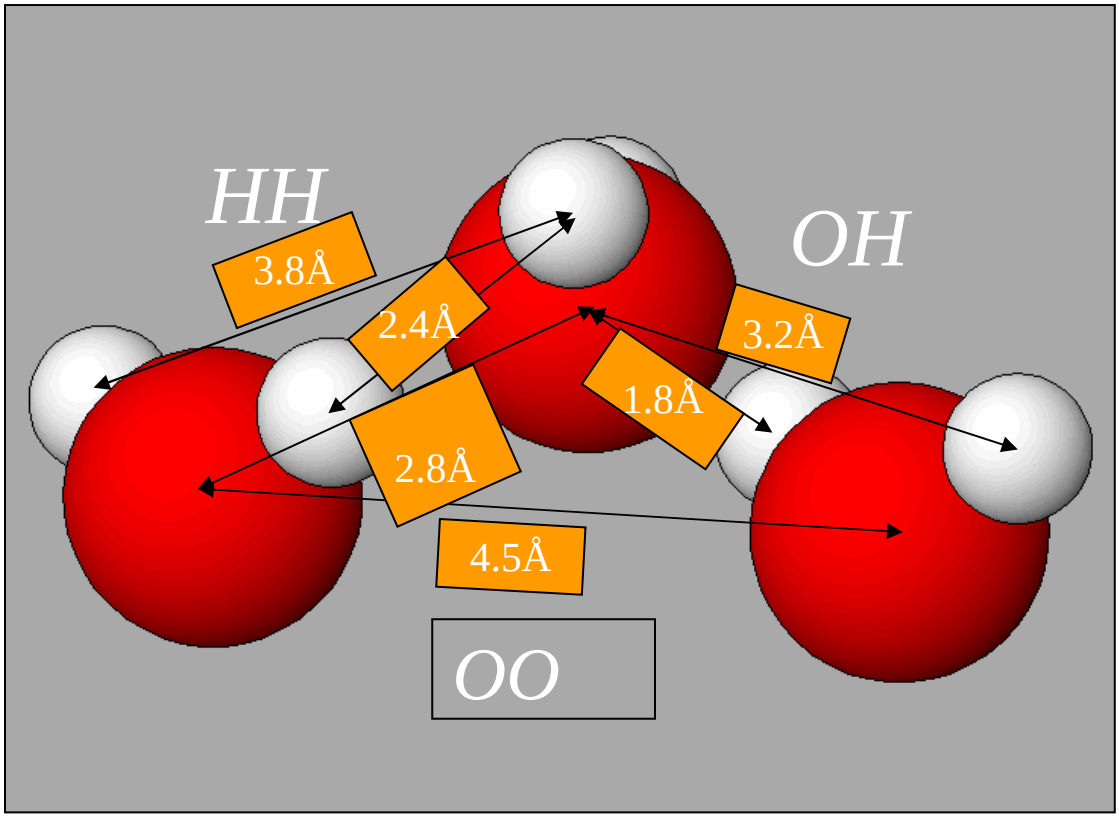

G 3.3d) The peak positions should compare reasonably closely with the distances shown above. The difference between a picture such as above and the real system is that the above gives a sketch of only the *average* local arrangement. The instantaneous distribution may look quite different – sometimes it is hard to recognise the hydrogen bond structure in water just by looking at boxes of molecules.

G 3.3e) How did you get on? Can you understand, on the basis of the sketch such as above the neighbouring water molecules lie in the directions they do?

G 3.3f) Note that the distance range shown does not include all of the second peak in the g_{OO} function, only the bit up to the maximum of the second peak. The obvious feature is that this second shell appears to be in almost exact antiphase with the first shell. This kind of alternating structure appears to be common to tetrahedral fluids.

G 3.3g) For lobe I the neighbour molecule tends to lie with its own *z*- axis pointing *away* from the central molecule, but there is fair amount of floppiness in this, with quite a lot of rotation about this axis possible. For lobe II the neighbour molecule has one of it H atoms pointing directly at the central molecule, but the rotation of the second H atom on this neighbour molecule is then poorly defined.

H: Polarized Neutrons

Answers H

H1. a) Flipping ratio: $F = N_+ / N_- = 51402 / 1903 =$ 27 +/- 0.6

$$\{error\ bar\ \ dF = \sqrt{\left(\frac{dN_+}{N_-}\right)^2 + \left(\frac{dN_-N_+}{N_-^2}\right)^2} \Rightarrow dF = 0.63\}$$

Therefore, the polarization is: $P = F - 1 / F + 1 =$ 0.929 +/- 0.002

$$\{error\ bar\ \ dP = \left(\frac{2}{(F+1)^2}\right)dF \Rightarrow dF = 0.002\ \}$$

b) Systematic errors in this measurement will largely arise from background contributions from the instrumental environment. In order to measure a reliable flipping ratio, the N_+ and N_- counts must be measured with and without the sample in the beam. The flipping ratio is then given by

$$F = \frac{N_+^{sample} - N_+^{empty}}{N_-^{sample} - N_-^{empty}}$$

Other sources of systematic error will be different values of the polarizing power of the polarizer and analyser, in addition to the finite flipping efficiency of the flipper.

H2. a) The adiabacity parameter is given by $E = \frac{\omega_L}{\omega_B}$

The Larmor frequency, $\omega_L = \gamma B$, where the gyromagnetic ratio, γ is given by the ratio of the neutron magnetic moment to its angular momentum ($=\frac{1}{2}\hbar$)

Therefore: $\omega_L = \frac{2\mu_n B}{\hbar} = 1.83 \times 10^8 B$ rad s^{-1} with B given in T.

In this example, B = 3 mT and is constant in magnitude, => $\omega_L = 5.49 \times 10^5$ rad s^{-1}

Now: $\omega_B = \frac{d\theta}{dy}.v = \frac{\pi/2}{0.1}.v = 15.71v$

Expressing *v* in terms of λ: $E = \frac{h^2}{2m_n\lambda^2} = \frac{m_n v^2}{2} \Rightarrow v = \frac{h}{m_n\lambda} = \frac{3956}{\lambda}$ with *v* in m s^{-1} and λ in Å.

So: $\omega_B = 15.71\frac{3956}{2} = 31074$ rad s^{-1}.

The adiabacity parameter is therefore: E = 17.7 and the field/flipper design should successfully propagate the neutron polarization and flip the spins without significant depolarization.

b) The design could be improved by either increasing the guide fields (and the current in the Dabbs foil) or by lengthening the distance over which the field rotates by 90°.

H3. a) The number of neutrons transmitted through an absorbing material is:
$n = n_0 \exp(-N\sigma t)$ where n_0 is the initial number of neutrons, N is the number density of atoms in the material, σ is the mean absorption cross-section and t is the thickness of the material. So the numbers of + and – neutrons transmitted is:

$n_+ = n_0 \exp(-N\sigma_+ t) = n_0 \exp(-N\sigma_0 t)\exp(-N\sigma_p t)$

$n_- = n_0 \exp(-N\sigma_- t) = n_0 \exp(-N\sigma_0 t)\exp(N\sigma_p t)$

Therefore the polarization is: $P = \frac{n_+ - n_-}{n_+ + n_-} = \frac{\exp(-N\sigma_p t) - \exp(N\sigma_p t)}{\exp(-N\sigma_p t) + \exp(N\sigma_p t)} = -\tanh(N\sigma_p t)$

The transmission of each spin state is: $T_\pm = \frac{n_\pm}{n_0} = \exp(N\sigma_\pm t)$

Therefore the total transmission:

$T = \frac{T_+ + T_-}{2} = \exp(-N\sigma_0 t)\frac{\exp(-N\sigma_p t) + \exp(N\sigma_p t)}{2} = \exp(-N\sigma_0 t)\cosh(N\sigma_p t)$

b) The expression for the spin-dependent absorption of a nuclear spin filter is $\sigma_\pm = \sigma_a(E)(1 \pm \rho P_N)$ where, P_N is the nuclear polarization and $\sigma_a(E)$ is the energy dependent absorption cross-section. The constant ρ is given by the expressions:

$\rho = \frac{I(1-2x) - x}{I+1}$, where $x = \frac{\sigma_{I-1/2}}{\sigma_{I+1/2} + \sigma_{I-1/2}}$.

Since ^{3}He absorbs only through the $I - ½$ channel, we may put $\sigma_{I+1/2} = 0$, and therefore: $\rho = -1$.

Therefore: $\sigma_\pm = \sigma_a(E)\left(1 \mp P_{He}\right) = \sigma_0 \pm \sigma_p$

So, equating the spin-independent and spin-dependent parts of the expression, we get

$\sigma_0 = \sigma_a(E)$

$\sigma_p = -\sigma_0 P_{He} \Rightarrow P_{He} = -\frac{\sigma_p}{\sigma_0}$

Substituting this back into the general expressions for the spin-filter polarization and transmission, we get:

$P = \tanh(P_{He} N\sigma_0 t)$ and $T = \exp(-N\sigma_0 t)\cosh(P_{He} N\sigma_0 t)$

H4. The expression for the differential cross-section from a magnetised crystal, with magnetisation direction $\hat{\boldsymbol{\eta}}$ perpendicular to the scattering vector **Q**, we have

$\frac{d\sigma}{d\Omega} = F_N^2(\mathbf{Q}) + 2F_N(\mathbf{Q})F_M(\mathbf{Q})\left[\mathbf{P}\cdot -\hat{\boldsymbol{\eta}}\right] + F_N^2(\mathbf{Q})$

Therefore the expressions for n_+ ($\mathbf{P}\cdot -\hat{\boldsymbol{\eta}} = -1$) and n_- ($\mathbf{P}\cdot -\hat{\boldsymbol{\eta}} = 1$) are

$$n_+ = \left(F_N - F_M\right)^2$$

$$n_- = \left(F_N + F_M\right)^2$$

Therefore, the polarization is: $P = \dfrac{\left(F_N - F_M\right)^2 - \left(F_N + F_M\right)^2}{\left(F_N - F_M\right)^2 + \left(F_N + F_M\right)^2} = \dfrac{-4F_N F_M}{2F_N^2 + 2F_M^2} = \dfrac{-2F_N F_M}{F_N^2 + F_M^2}$

The minus sign indicates that the neutrons are polarized antiparallel to the direction of magnetisation of the crystal.

H5. The first rule of thumb in magnetic polarized neutron scattering is that spin-flipped neutrons will only be produced by components of the sample magnetisation perpendicular to the neutron polarization direction. [This is an extremely useful rule to bear in mind during all polarized neutron experiments.] Therefore, if we are scattering neutrons from a fully magnetised scatterer (i.e. a ferromagnet for example) – magnetised in the direction of the neutron polarization (which is an experiment necessity), then there will be no perpendicular components of the magnetisation, and therefore no spin-flip scattering. We can therefore dispense with the analysers, since the scattered beam remains fully polarized.

H6. a) The Pauli spin relations are:

$$\sigma_x|\uparrow\rangle = \begin{bmatrix}0 & 1\\ 1 & 0\end{bmatrix}\cdot\begin{bmatrix}1\\0\end{bmatrix} = \begin{bmatrix}0\\1\end{bmatrix} = |\downarrow\rangle$$

$$\sigma_x|\downarrow\rangle = \begin{bmatrix}0 & 1\\ 1 & 0\end{bmatrix}\cdot\begin{bmatrix}0\\1\end{bmatrix} = \begin{bmatrix}1\\0\end{bmatrix} = |\uparrow\rangle$$

$$\sigma_y|\uparrow\rangle = \begin{bmatrix}0 & -i\\ i & 0\end{bmatrix}\cdot\begin{bmatrix}1\\0\end{bmatrix} = i\begin{bmatrix}0\\1\end{bmatrix} = i|\downarrow\rangle$$

$$\sigma_x|\downarrow\rangle = \begin{bmatrix}0 & -i\\ i & 0\end{bmatrix}\cdot\begin{bmatrix}0\\1\end{bmatrix} = -i\begin{bmatrix}1\\0\end{bmatrix} = -i|\uparrow\rangle$$

$$\sigma_z|\uparrow\rangle = \begin{bmatrix}1 & 0\\ 0 & -1\end{bmatrix}\cdot\begin{bmatrix}1\\0\end{bmatrix} = \begin{bmatrix}1\\0\end{bmatrix} = |\uparrow\rangle$$

$$\sigma_z|\downarrow\rangle = \begin{bmatrix}1 & 0\\ 0 & -1\end{bmatrix}\cdot\begin{bmatrix}0\\1\end{bmatrix} = -\begin{bmatrix}0\\1\end{bmatrix} = -|\downarrow\rangle$$

b) Now, we have to calculate the matrix element for magnetic scattering $\langle S'|V_m|S\rangle$, where $S`$ and S are the final and initial spin states, and V_m is the magnetic interation potential, which is given by

$$V_m = \frac{-\gamma_n r_0}{2m_n}\sum_\zeta \sigma_\zeta M_{\perp\zeta}$$

Therefore, the 4 possible spin-transitions are given by

i) Non-spin-flip: $|\uparrow\rangle \rightarrow |\uparrow\rangle$

$$\langle\uparrow|V_m|\uparrow\rangle = \frac{-\gamma_n r_0}{2m_n}\left(\langle\uparrow|\sigma_x|\uparrow\rangle M_{\perp x} + \langle\uparrow|\sigma_y|\uparrow\rangle M_{\perp y} + \langle\uparrow|\sigma_z|\uparrow\rangle M_{\perp z}\right)$$

$$= \frac{-\gamma_n r_0}{2m_n}\left(\langle\uparrow|\downarrow\rangle M_{\perp x} + i\langle\uparrow|\downarrow\rangle M_{\perp y} + \langle\uparrow|\uparrow\rangle M_{\perp z}\right)$$

$$= \frac{-\gamma_n r_0}{2m_n} M_{\perp z}$$

ii) Non-spin-flip: $|\downarrow\rangle \rightarrow |\downarrow\rangle$

$$\langle\downarrow|V_m|\downarrow\rangle = \frac{-\gamma_n r_0}{2m_n}\left(\langle\downarrow|\sigma_x|\downarrow\rangle M_{\perp x} + \langle\downarrow|\sigma_y|\downarrow\rangle M_{\perp y} + \langle\downarrow|\sigma_z|\downarrow\rangle M_{\perp z}\right)$$

$$= \frac{-\gamma_n r_0}{2m_n}\left(\langle\downarrow|\uparrow\rangle M_{\perp x} - i\langle\downarrow|\uparrow\rangle M_{\perp y} - \langle\downarrow|\downarrow\rangle M_{\perp z}\right)$$

$$= \frac{-\gamma_n r_0}{2m_n}\left(-M_{\perp z}\right)$$

iii) Spin-flip: $|\uparrow\rangle \rightarrow |\downarrow\rangle$

$$\langle\uparrow|V_m|\downarrow\rangle = \frac{-\gamma_n r_0}{2m_n}\left(\langle\uparrow|\sigma_x|\downarrow\rangle M_{\perp x} + \langle\uparrow|\sigma_y|\downarrow\rangle M_{\perp y} + \langle\uparrow|\sigma_z|\downarrow\rangle M_{\perp z}\right)$$

$$= \frac{-\gamma_n r_0}{2m_n}\left(\langle\uparrow|\uparrow\rangle M_{\perp x} - i\langle\uparrow|\uparrow\rangle M_{\perp y} - \langle\uparrow|\downarrow\rangle M_{\perp z}\right)$$

$$= \frac{-\gamma_n r_0}{2m_n}\left(M_{\perp x} - iM_{\perp y}\right)$$

iv) Spin-flip: $|\downarrow\rangle \rightarrow |\uparrow\rangle$

$$\langle\downarrow|V_m|\uparrow\rangle = \frac{-\gamma_n r_0}{2m_n}\left(\langle\downarrow|\sigma_x|\uparrow\rangle M_{\perp x} + \langle\downarrow|\sigma_y|\uparrow\rangle M_{\perp y} + \langle\downarrow|\sigma_z|\uparrow\rangle M_{\perp z}\right)$$

$$= \frac{-\gamma_n r_0}{2m_n}\left(\langle\downarrow|\downarrow\rangle M_{\perp x} + i\langle\downarrow|\downarrow\rangle M_{\perp y} + \langle\downarrow|\uparrow\rangle M_{\perp z}\right)$$

$$= \frac{-\gamma_n r_0}{2m_n}\left(M_{\perp x} + iM_{\perp y}\right)$$

These equations show that the magnetic non-spin-flip scattering is entirely due to the component of the magnetisation parallel to the neutron polarization direction, $M_{\perp z}$; and that the magnetic spin-flip scattering is entirely due to the components of the magnetisation perpendicular to the neutron polarization direction, $M_{\perp x}$ and $M_{\perp y}$.

H7. From the previous question (which is a derivation of the magnetic part of the Moon, Riste and Koehler equations) we have established that spin-flip scattering arises solely from the components of the sample magnetisation perpendicular to the neutron polarization.
Now, the definition of the neutron sensitive sample magnetisation is $M_{\perp}(\mathbf{Q}) = -2\mu_B\left[\boldsymbol{\eta} - (\boldsymbol{\eta}\cdot\hat{\mathbf{Q}})\hat{\mathbf{Q}}\right]$ where $\boldsymbol{\eta}$ is the sample magnetisation (see, for example, Squires, or previous lectures on magnetic scattering).
From this equation, we note that if the scattering vector is parallel to the sample magnetisation, then the neutron sensitive magnetisation is zero.

Therefore, if the neutron polarization is parallel to the scattering vector, the only components of the magnetisation that will scatter neutrons will be perpendicular to the polarization, and will therefore flip the neutron spins.

H8. The advantage of the X-Y-Z difference method of magnetic scattering separation over the method of measuring with the neutron polarization **P** || **Q**, is that the X-Y-Z method applies to a general multi-detector instrument. The **P** || **Q** method only works for one scattering vector at a time.

A further advantage of X-Y-Z is that it is insensitive to background, since the spin-flip background will be the same in Z, X and Y directions, and will therefore cancel out.

H9. The technique of neutron spin-echo, relies on the fact that the neutrons experience an equal and opposite field integral on both side of the sample, so that the neutron spins re-phase precisely. In practice this is achieved by a Mezei π-flipper placed just before the sample. This rotates the de-phased neutron spin "disc" by 180 degrees around its horizontal axis. If the sample is a paramagnet, then the magnetic scattering will rotate *exactly half* of neutrons in the de-phased spin "disc" by 180 degrees around its horizontal axis. The other, non-rotated half of the magnetic signal, along with the nuclear and spin-incoherent signal, will be lost (not re-phased).

Therefore, the advantage of NSE over, e.g. backscattering techniques, is that the magnetic signal is automatically selected and separated from other components of the scattering.